Implications for Focused Fluid Transport at the Northern Cascadia Accretionary Prism From a Correlation between BSR Occurrence and Near Seafloor Reflectivity Anomalies Imaged in a Multi-Frequency Seismic Data Set

Lars Zühlsdorff, Volkhard Spieß, Christian Hübscher,
Heinrich Villinger, Andreas Rosenberger

Universität Bremen
Fachbereich Geowissenschaften

Corresponding author:

Lars Zühlsdorff
Fachbereich 5 - Geowissenschaften
Universität Bremen
Postfach 33 04 40
28334 Bremen
Tel.: 0421 218 7184
Fax.: 0421 218 7179
email: lzuehls@mtu.uni-bremen.de

Keywords: Cascadia accretionary prism, very high resolution seismics, fluid migration, bottom simulating reflector, near surface reflectivity anomalies

Abstract

A high resolution seismic survey was carried out at the accretionary prism on the continental slope off Vancouver Island, Canada. Two GI-Gun data sets with different source frequency ranges of 50-150 Hz and 100-500 Hz were combined with 4 kHz narrow beam echosounding data (Parasound). The data allow spatial correlation between a gas hydrate bottom simulating reflector (BSR) and distinct areas of high near seafloor reflectivity. An integrated interpretation of the multi-frequency data set provides insight into the regional distribution of tectonically induced fluid migration and gas hydrate formation in the vicinity of ODP Leg 146 Sites 889 and 890.

The BSR at the base of the gas hydrate stability field is observed within accreted and deformed sediments, but appears to be absent within bedded slope basin deposits. It is suggested that these basin deposits inhibit vertical fluid flow and prevent the formation of a BSR, whereas the hydraulic conductivity of the accreted sediments is sufficiently high to allow for pervasive gas migration. An elevation of the BSR beneath the flanks of a topographic high is interpreted as an indicator for local upflow of warm fluids along permeable pathways within outcropping accreted sediments.

Parasound data reveal discontinuous zones of high reflectivity at or directly beneath the seafloor, which may indicate local cementation of surface sediments. In combination with GI-Gun data, the occurrence of these reflective areas can be related to the location of slope sedimentary basins acting as hydraulic seals. It is proposed that the seals sometimes fail along faults extending beneath the BSR, leading to focused upflow of methane bearing fluid and the formation of carbonate pavements at the seafloor.

Introduction

Gas hydrate is an ice-like substance which is formed at high pressure and low temperature, consisting of a lattice of water molecules with cages containing guest gaseous molecules bonded by Van der Waals forces (e.g. Sloan 1990; MacKay et al. 1994). The most common hydrate forming gas is methane (e.g. Claypool and Kaplan 1974). Since hydrates may store enormous quantities of methane in marine sediments, they are important as a possible clean energy source, may affect atmospheric composition and global climate change, and represent a potential submarine geologic hazard by decreasing the stability of slope sediments (Kvenvolden 1988; Kvenvolden 1994).

The stability conditions for solid hydrate mainly depend on temperature and pressure, and, to a lesser extent, on the composition of hydrate forming constituents and the salinity of the pore fluid (e.g. Sloan 1990). Since the subbottom depth to the base of the stability field is more strongly a function of temperature than of pressure, the base of solid hydrates approximately marks an isotherm. The associated seismic signature is a bottom-simulating reflector (BSR), because isotherms generally follow the seafloor, except where local changes of the temperature gradient are present (e.g. Hyndman and Davis 1992; Kvenvolden 1994). The BSR can be interpreted either as the top of a low velocity zone caused by free gas beneath the layer (Singh et al. 1993), or as the base of a high velocity layer of hydrate-cemented sediments above (Hyndman and Davis 1992). In many cases, however, the effect of hydrate and free gas appear to combine.

The common concentrations of organic matter in marine sediments are probably insufficient to locally generate the large volumes of methane needed for the formation of significant amounts of hydrate (e.g. Claypool and Kaplan 1974; Paull

et al. 1994). Alternatively, hydrates may form either through dissociation of pre-existing hydrate, if the base of the stability field moves upward (e.g. Dillon and Paull 1983; Kastner et al. 1995), or methane originating at greater depth is transported by upward pore fluid migration (Hyndman and Davis 1992). Even when the effects of in situ production and upward migration of methane on hydrate formation may also combine, some kind of vertical fluid transport appears to be essential (Paull et al. 1994; Gornitz and Fung 1994).

The occurrence of gas hydrate may therefore be diagnostic of upward fluid flow (Hyndman and Davis 1992). Further, local upward flow along permeable conduits was inferred from variations of BSR subbottom depth, which indicate local changes of the temperature gradient (e.g. Minshull and White 1989; Davis et al. 1995). More evidence for upward migration of pore fluids in accretionary prisms was provided through seismic estimates of porosity reduction (e.g. Bray and Karig 1985; Minshull and White 1989; Calvert and Clowes 1991), by studies of the physical and thermal states of the sediments (e.g. Davis et al. 1990; Hyndman et al. 1993; Sample and Kopf 1995), and by mapping and sampling of early diagenetic deposits near the seafloor (e.g. Ritger et al. 1987; Kulm and Suess 1990; Carson et al. 1994).

Ever since dewatering processes at accretionary prisms were first investigated, some questions have remained, including the magnitude of flow, the modulation of flow rates over time and the relative importance of focused flow versus diffuse flow (Suess et al. 1998). Upflow velocities along faults were suggested to be 2 to 3 orders of magnitude higher than dispersed flow through the sediment (Moore et al. 1990), but dispersed flow, accommodated by intergranular and small scale fracture permeability, leaks out over much larger areas and thereby causes an

unknown proportion of water loss (e.g. Carson and Screaton 1998). An accurate estimate of mass transport rates is further hampered by the effect of transient processes, since fluid expulsion may be coupled to episodic fault displacement and to the earthquake cycle (Moore and Vrolijk 1992). Hence, the distribution and nature of flow must be determined at any study area before a quantitative estimate of the fluid budget becomes possible.

At the northern Cascadia accretionary prism, tectonic loading rather than tectonic compression may be the most important factor controlling excess pore pressure generation and fluid migration (Hyndman and Davis 1992; Moran et al. 1995). Approximately 3.5 km of Cascadia Basin sediment is almost completely scraped off the downgoing Juan de Fuca plate, and the thickness of the sediment wedge doubles over a distance of only 10-20 km from the deformation front (e.g. Davis and Hyndman 1989; Hyndman and Davis 1992). One consequence of this tectonic thickening is rapid porosity loss with depth, associated with the expulsion of large volumes of fluids (e.g. Davis et al. 1990). ODP Leg 146 was directed to the investigation of this fluid flow and sediment deformation at the Cascadia Margin (Shipboard Scientific Party 1994).

In this study, fluid transport processes in the vicinity of ODP Leg 146 Sites 889 and 890 are investigated in greater detail. Both seafloor and subbottom features related to fluid flow are imaged in a multi-frequency seismic data set providing sufficient resolution at each depth level. Distinct areas of high seafloor reflectivity observed in Parasound data are related to seismic observations of a gas hydrate BSR. This provides insight into the regional distribution of diffuse and confined tectonically induced fluid migration and gas hydrate formation.

Study area

Ten lines of single channel and multi channel seismic data were collected within an area of about 15 by 15 km in the vicinity of ODP Sites 889 and 890 (Leg 146). The drill sites are located on the continental slope off Vancouver Island in water depths of 1315 m and 1326 m, respectively (Fig. 1). At both locations, the pervasively fractured and folded material of the accretionary wedge is covered by a veneer of stratified slope sediments. They appear to consist predominantly of turbidites and hemipelagic deposits (Shipboard Scientific Party 1994). Figure 1 shows part of a 20-km-wide gently undulating plateau, where accreted sediments locally crop out. A steep escarpment to the west separates the plateau from the lower slope.

Within the study area, the absence of major thrust faults, as well as the lack of significant thermal anomalies, suggest diffuse dewatering hosted by intergranular permeability (e.g. Hyndman and Davis 1992; Kastner et al. 1995). At the location of the ODP sites, however, a linear temperature decrease with depth implies conductive heat loss rather than advection, although upward fluid movement at rates of about 1 mm/a cannot be excluded (Shipboard Scientific Party 1994). Unfortunately, the ODP packer experiment at Site 889 (Circulation Obviation Retrofit Kit, CORK) failed due to technical problems, and in situ hydrogeologic data of dispersed flow and discharge are not available (Carson and Westbrook 1995).

Data acquisition and processing

The seismic survey was carried out during R/V Sonne Cruise SO111 in late summer 1996 (Villinger et al. 1996). Single channel data along Lines 1 to 7 (Fig.

1) and multi channel data (Lines GeoB96-069, GeoB96-071 and GeoB96-073) were collected, providing images of the complete sediment section down below BSR depth. Simultaneously, two hydro-acoustic systems were operated along all seismic lines, imaging the upper part of the sediment column at very high resolution (Parasound) and providing a map of seafloor bathymetry (Hydrosweep). Some details about data acquisition and processing are listed below:

(1) Single channel seismics (scs): All 16 hydrophone groups of a 100 m long Teledyne streamer were stacked. A GI-Gun with 0.7 l main chamber volume and 1.7 l secondary chamber volume (GI-Gun #1) provided a frequency range of about 50-150 Hz. A shot rate of 10 s corresponded to a shot spacing of 25 m.

(2) Multichannel seismics (mcs): A 300 m long Syntron streamer, equipped with separately programmable hydrophone subgroups, was optimized for the given water depth of >1100 m using 24 groups at a length of 6.25 m. Four remotely controlled birds kept the streamer depth within a range of 1 m, and magnetic compass readings allowed to determine the position of each streamer group relative to the ship's course. A GI-Gun with 2 x 0.4 l chamber volume (GI-Gun #2) generated signal frequencies between 100 and 400 Hz.

(3) Hydro-acoustic systems: a) Depending on the type of sediment, the narrow beam Parasound echosounder (4 kHz, opening angle 4°) may penetrate up to 100 m of the sediment column. Seafloor reflections can be recorded for bedding inclinations up to 2°. b) The Hydrosweep multibeam swath-sounder was used to map the seafloor bathymetry as displayed in Figure 1.

Standard processing for single channel and multi channel seismic data (Tab. 1) was carried out with the Seismic Unix software package (Stockwell 1997). For the multi channel data, additional custom software was developed to correct for

streamer towing depth and to determine geographic positions of CDP (common depth point) bins at a spacing of 10 m.

A seismic velocity model is needed for normal move-out correction (mcs) and time migration (scs and mcs). Therefore, velocity analysis was applied to the three multi channel lines. Due to the short streamer length, however, an error of about 10% was expected for the estimated seismic velocities. Since observed velocity variations appear to be small, a constant velocity of 1750 m/s for stacking and migration was assumed for all lines within the study area. This is in good agreement with average velocities from VSP data (ODP Site 889, MacKay et al. 1994) and from a full waveform inversion of mcs data (Yuan et al. 1996). Both data sets reveal a velocity increase from 1700 m/s to 1900 m/s in the 100 m depth interval above the BSR. This increase was attributed to a hydrate concentration of 20% of pore space just above the BSR (e.g. Hyndman and Spence 1992; Yuan et al. 1996). However, since the implications and conclusions of this study are only based on relative changes of reflector strength and subbottom depth, the choice of a constant velocity model for data analysis produces negligible errors.

Observations

Within all GI-Gun data sets, the accreted and deformed material of the accretionary wedge is characterized by a total lack of coherent reflection energy. Therefore, the prism sediments can be easily distinguished from sedimentary basins, which contain stratified hemipelagic deposits (Fig. 2a-5a).

A clear BSR with negative reflection polarity occurs mainly within accreted sediments at a two-way reflection time (TWT) of about 275 ms below seafloor. For the lower frequency GI-Gun #1, the amplitudes of the BSR and the seafloor

reflection are of the same order (Fig. 2a). In contrast, the BSR amplitude for the higher frequency GI-Gun #2 is just above the noise level and much smaller than the sea floor return (Fig. 3a). For both sources, the BSR appears to be discontinuous. In Figure 4a, the BSR is not present between shot numbers 1 and 150 and between shot numbers 505 and 540. In both areas, basins of stratified sediments are deeper than the BSR. Figure 5a shows a close-up of the northern half of Line 3, which is also dominated by bedded deposits. The BSR can be identified in the vicinity of shot number 255, where the sediment section is cut by a fault, but it can not be traced throughout the basin. All seismic lines within the study area consistently indicate that the BSR is not observed within basins of bedded deposits, except where vertical or subvertical structures as faults are present (e.g. Fig. 5a). In contrast, the BSR is always observed within the pervasively fractured sediments of the accretionary prism.

Parasound data reveal up to 8 m thick zones of high reflectivity at or directly beneath the seafloor, which are not imaged at the wavelengths provided by both GI-Guns (Fig. 2b-5b). The zones are discontinuous and covered by a 0.5-5 m thick transparent sediment drape as shown in a close-up of the Parasound record of Line GeoB96-071 (Fig. 6). Both, the high surface reflectivity and the kind of draping, are not typical for sediments of the Cascadia Basin (Villinger et al. 1996). Figure 6 also indicates that zones of high reflectivity follow the layering in the top portion, but do not reveal a sharp base. In addition, they are much thicker than the commonly observed bedded layers.

A comparison of Parasound records with GI-Gun data shows that intervals of strong surface reflectivity appear only in the vicinity of sedimentary basins (Fig. 2-5). Furthermore, the occurrence of high seafloor reflectivity may be related to

the occurrence of the BSR. For all lines, the locations, where a clear BSR could be identified (Fig. 7a), and zones of high seafloor reflectivity (Fig. 7b) were mapped. The overall pattern presented in Figure 7 seems to indicate that the presence of a BSR and of strong surface reflections is mutually exclusive. This relationship is most evident for the basin at the north-eastern corner of the study area, where bedded deposits are deeper than the expected depth of the BSR (Fig. 4-5). One exception, where both features are present, is a small area at the northern flank of a topographic high near ODP Site 889, where sedimentary basins are shallower than the BSR (Fig. 2-3).

Zones of high seafloor reflectivity, however, are not present in all sedimentary basins. GI-Gun data suggest that their occurrence may be related to the sediment structure underneath. Two types of faults, which frequently cut the bedded sediment section, can be observed: (a) growth faults (e.g. Fig. 2a at shot number 570, Fig. 4a at shot number 475), and (b) normal faults, which may cause several meters of vertical displacement throughout the sediment column down to >200 m subbottom depth (e.g. Fig. 4a at shot numbers 25 and 445, Fig. 5a at shot number 255). A comparison with Parasound data indicates that the occurrence of high near seafloor reflectivity may be coupled to the presence of those normal faults.

In Figure 8, a close-up of the deformed and faulted zone in Figure 2a (shot number 310), which is located at the northern flank of a topographic high, is displayed after leveling the first arrivals. The seafloor topography as well as the location of high amplitude reflectors are given in the corresponding Parasound section. A structural disturbance of the sediment column is associated with intervals of high reflectivity at the seafloor. In addition, the BSR at this location is elevated and interrupted by a gap of about 300 m width.

To determine the BSR-topography, i.e. the TWT distance to the sea floor, a map was created by leveling the seafloor reflection for all lines and then picking the two-way reflection time for the BSR. The values were gridded using algorithms of the GMT software package (Smith and Wessel 1990) and plotted as grey shades of positive or negative deviation from the mean BSR depth below seafloor (Fig. 9a). Furthermore, grey shades indicating BSR-topography were related to contour levels of the seafloor bathymetry (Fig. 9b), suggesting that the BSR is elevated at distinct areas which correspond to the flanks of topographic highs. The maximum elevation of about 50 ms TWT (corresponding to 44 m for an assumed average velocity of 1750 m/s) is found in the small area where both a BSR and a zone of high surface reflectivity are observed, and a significant structural disturbance of the sediment column is present (Fig. 2 and Fig. 8).

Discussion

1. Nature of the BSR

In the following discussion, the BSR is considered to mark the base of the gas hydrate stability field. This is in agreement with results from previous studies, indicating a small amount of free gas beneath a zone with 10-20% of the pore spaces filled with hydrate (Hyndman and Spence 1992; Shipboard Scientific Party 1994; Kastner et al. 1995; Spence et al. 1995; Yuan et al. 1996). Thus, the base of the hydrate layer is characterized by a relatively sharp decrease of seismic impedance and produces a BSR with reversed reflection polarity (Fig. 2a-5a).

The top of the hydrate zone as well as the base of the gas layer appear to be very gradational, since no reflections can be observed even at low frequencies (Spence et al. 1995; Fink and Spence 1999). In addition, VSP data from ODP Site 889

indicate that the transition between hydrate cemented sediment and the gas layer below may also be gradational within a small depth interval of less than 20 m (MacKay et al. 1994). This may explain the relative decrease of the BSR amplitude for the higher frequency signal of GI-Gun #2 (multi channel seismics). A lower BSR amplitude for higher frequency signals is consistent with results of previous studies suggesting that the BSR amplitude is frequency dependent (Spence et al. 1995; Fink and Spence 1999). An alternative explanation for a weak BSR in the multi channel data could be seismic attenuation. However, layers of bedded sediments still produce strong reflection amplitudes at the depth of the BSR (Fig. 3a), implying that weak BSR amplitudes are related to interference effects rather than to an overall attenuation of reflected energy.

2. BSR distribution and subbottom depth

With the exception of faulted zones as shown in Figure 5a, no distinct BSR is observed within the slope sedimentary basins (Fig. 2a-5a). Instead, the internal reflectors, which are commonly parallel or subparallel to the seafloor, reveal high reflection amplitudes. It was therefore suggested by Spence et al. (1995) that the BSR is still present, but may be obscured by stronger reflectors. However, the BSR is of chemical nature and is not expected to be related to the layering. Thus, it should be visible wherever other reflectors are inclined with respect to the seafloor. This is not in agreement with the data presented in this paper (e.g. Fig. 4a, shot numbers 100-200).

Hence, the most likely explanation for the absence of the BSR in sedimentary basins is an insufficient concentration of gas and gas hydrate. Since the local production of gas in marine sediments does generally not support the formation of

hydrates (e.g. Claypool and Kaplan 1974), it was suggested that the occurrence of a BSR implies diffuse upward migration of gas or gas-saturated fluid (Hyndman and Davis 1992). Then, the absence of a BSR within basins of bedded deposits indicates that gas is not provided at sufficient rates.

It is therefore inferred that the bedded hemipelagic deposits inhibit significant vertical flow, whereas the pervasively fractured and permeable sediments of the accretionary prism accommodate diffuse fluid and gas migration. Consequently, the BSR should be disrupted, wherever the low permeable sedimentary basins are deeper than the base of the hydrate stability field (Fig. 4a-5a). Rising gas or fluid from below may then be diverted to the sides, following the interface between the basins and the accreted sediments towards the closest permeable conduit. A local formation of hydrate in the vicinity of faults may thereby be explained by confined gas or fluid migration (e.g. Fig. 5a, shot number 255).

The topography of the BSR was mapped in Figure 9, showing a distinct shallowing which corresponds to a zone beneath the northern flank of a topographic high (Fig. 9b). In principle, this effect could be caused by a difference in seismic velocity between accreted sediments and slope basin deposits. However, no significant lateral variation of BSR depth is observed when the thickness of the bedded section laterally changes. One example is found in the southern part of Figure 4, where the BSR depth is not affected by the slowly increasing thickness of the bedded deposits above. This suggests that seismic velocities of accreted and bedded sediments are almost similar. Furthermore, VSP data from ODP Site 889 reveal velocities between 1700 and 1900 m/s in the accreted sediments above the BSR (MacKay et al. 1994), which are not significantly higher than the basin velocity of about 1750 m/s estimated from GI-

Gun data.

Alternatively, an elevation of the BSR is expected when either the thermal conductivity of the sediments or one or more of the parameters controlling hydrate stability have changed. However, thermal conductivity is assumed to be constant, since no significant change between bedded and accreted sediments was observed at ODP Sites 889 and 890 (Shipboard Scientific Party 1994). Further, effects such as a local pressure decrease, local variations of salinity, or a changing composition of hydrate forming constituents may considered to be of minor importance, since hydrate stability is more sensitive to temperature variations. BSR elevations with respect to the seafloor may then be best explained by a local upflow of warm fluids, which increases the temperature gradient and rises the isotherm imaged by the BSR. Similar effects were described by Minshull and White (1989) for the Makran accretionary prism and modeled by Davis et al. (1995) for the Cascadia prism off Oregon.

On the basis of a temperature gradient of 54°C/km and a constant thermal conductivity of 1.15 W/(mK) (Shipboard Scientific Party 1994), the depth of the BSR was used to estimate a conductive heatflow of 62 mW/m² at areas of average BSR depth. The error of this estimate may be as high as 10% due to uncertainties in seismic velocity and temperature at the BSR. However, it is in agreement with a value of 62+/-8 mW/m² given at ODP Sites 889 and 890 (Shipboard Scientific Party 1994). Referring to this as an average heatflow and assuming constant temperatures at the BSR, a positive heatflow anomaly of 18% may be expected in the area of maximum BSR elevation. Considering the fact that the temperature at the BSR may be lower at shallower depth and that estimation errors may be high, the heatflow anomaly may reduce to 10-15%.

As a result, a higher hydraulic conductivity favouring local thermally efficient upflow is inferred beneath the flanks of topographic highs. Although most fluid is thought to be expelled via distributed permeability, a part of the fluid loss within the study area therefore appears to be focused. However, a local variation of the regional geothermal gradient can only develop if the flow occurred recently and rapidly enough that thermal diffusion did not yet dissipate the anomaly (Fisher and Hounslow 1990; Davis et al. 1995). Since it must be assumed that local rates of focused flow may well be coupled to episodes of tectonic movement, flow rates may be time-dependent and the time-average of flow is expected to be lower than it may be estimated from recent thermal anomalies (e.g. Carson and Screaton 1998).

3. Near surface features

Figure 7b indicates that high reflectivity zones near the surface of sedimentary basins are not exclusively found at local depressions and do also occur at the flank of the topographic high near ODP Site 889. Furthermore, they are much thicker than the commonly observed bedded layers and do not reveal a sharp base (Fig. 6). Consequently, it is very unlikely that this kind of high surface reflectivity is related to sedimentary processes as the deposition of turbidites.

An increase in surface reflectivity may on the other hand be associated with early diagenetic processes as the cementation of surface sediment, which could increase acoustic impedance significantly. In principle, also layered gas hydrates of sufficient concentration may have a major impact on acoustic impedance. However, the BSR is not present within the sedimentary basins and distributed vertical gas migration is probably not sufficient for hydrate formation in bedded

surface layers. Thus, distinct hydrate layers which extend over larger areas near the seafloor are not likely to be expected.

Another early diagenetic product previously described at the Cascadia margin are carbonate cements (e.g. Kulm and Suess 1990; Kopf et al. 1995; Suess et al. 1998), which were attributed to the exposure of dissolved hydrocarbons to the low-temperature and low-pressure oxidizing conditions near the seafloor (e.g. Ritger et al. 1987, Carson et al. 1994). Carbonates may precipitate when the solubility of hydrocarbon constituents in a rising fluid decreases in response to hydrostatic pressure decrease, or excess carbonate is generated by microbial methane oxidation (e.g. Kulm and Suess 1990; Kopf et al. 1995; Suess et al. 1998). This suggests that carbonate formation near the seafloor is often directly related to focused pore water expulsion (e.g. Ritger et al. 1987).

From the arguments given above, pore water expulsion seems to be inhibited by pronounced bedding. However, ongoing tectonic activity as the compression of the accretionary prism or major earthquakes could trigger the failure of the stratigraphic seal. Faults may then create permeable pathways between the free gas layer below the BSR depth and the surface. The rise of pore fluid and free gas is associated with an expansion of free gas, thereby increasing buoyancy forces and accelerating the upflow. Under these circumstances, gas and fluid from greater depth can rapidly mix with bottom water, resulting in chemical reactions and precipitation. Cementation of seafloor sediment layers may then cause the higher acoustic reflectivity observed in Parasound data.

Based on echosounding data, this hypothesis can not be proved in detail. It is, however, supported by seismic observations of closely spaced faults, which cut the bedded sediments (Fig. 2a-5a). A fast release of pore fluids and a subsequent

distribution by currents and tidal forces may further explain why zones of high reflectivity often extend over distances of about 2 km around possible vent sites (Fig. 2b-5b). At the northern flank of the topographic high near ODP Site 889, Fink and Spence (1999) also described unusually high reflection coefficients at the surface within an area of about 2 km in diameter. Their analysis of synthetic seismograms revealed layer velocities and densities corresponding to those of carbonate (Fink and Spence 1999). Other studies documented disseminated carbonates throughout the sediment section at ODP Sites 889 and 890 (e.g. Shipboard Scientific Party 1994; Kopf et al. 1995), although no information was available directly from the sediment surface. Hyndman et al. (1994) assumed sandy layers containing carbonates to explain the low penetration of heatflow probes around ODP Site 889. Carson et al. (1994) mapped carbonate crusts in the vicinity of incipient thrust faults seaward of the deformation front off Oregon. They also derived that the seismic impedance of the crusts is about 4-6 times higher than for hemipelagic sediments, and that they may extend for distances of more than 250 m.

Fault controlled fluid discharge through low permeable sedimentary basins is therefore assumed to explain zones of high near seafloor reflectivity. Since major thrustfaults are absent in the study area, focused upflow is mainly related to local processes. Local tectonism creates topographic depressions, which are subsequently filled with bedded hemipelagic deposits. Growth-faults are active over long periods of time and reflect the development of those sedimentary basins. However, they would not allow for continuous focused flow due to their limited vertical extent of faulting during the intermittent tectonic activity. It is more likely that episodic fault displacement along the observed normal faults, which affects

the complete sediment column between the seafloor and the BSR, triggers single events of fluid expulsion, followed by periods, when the basin deposits act as an efficient seal. This is in agreement with the presence of a sediment drape, which must have been deposited after such an event (Fig. 2b-5b). On the other hand, permeable connections to the seafloor must be maintained sufficiently long to allow for the creation of thick cemented zones. The thickness of cemented intervals could be potentially used to determine the duration and intensity of confined fluid release.

As a result, indications for two different types of transient focused fluid flow are present in the study area, namely episodic upflow beneath the flanks of topographic highs and fault controlled discharge at sedimentary basins. The associated time scales do not necessarily have to be identical. However, the observations of Figure 8 suggest, that the same tectonic event may have initiated focused upflow beneath the flank of the topographic high near ODP Site 889 as well as confined fluid release through the bedded sediments above. The elevation of the BSR with respect to the seafloor, in conjunction with the interruption by a 300 m wide gap, implies that rising warm fluids may have decomposed solid hydrates. Zones of high surface reflectivity around the vent location are in agreement with a recent study suggesting that carbonate formation at the surface and dissociation of gas hydrates may be related (Bohrmann et al. 1998).

A quantitative estimate of rates of flow and mass exchange requires numerical modeling, which is beyond the scope of this paper. However, before flow can successfully be modeled, the thermal and hydraulic parameters as well as the nature and distribution of flow have to be determined. This seismic survey imaged local patterns of fluid discharge and provided a conceptual model for the fluid

regime in the vicinity of ODP Sites 889 and 890, which can be used to further constrain future investigations and models.

Summary and conclusion

From previous studies and ODP Leg 146 it was known that significant volumes of gas hydrates are present at the northern Cascadia accretionary prism. The base of the hydrate zone is marked by a BSR, which can be traced within the accreted and deformed material of the sedimentary wedge. In addition, the existence of a BSR may be diagnostic of dispersed fluid flow. The fluid release of this area is in general considered to be mainly accommodated by intergranular permeability.

In this study, two GI-Gun data sets with different source frequency ranges are combined with narrow beam echosounding data and the seafloor bathymetry provided by the Hydrosweep system. An integrated interpretation provides insight into the regional distribution of tectonically induced fluid migration and gas hydrate formation in the vicinity of ODP Leg 146 Sites 889 and 890.

The thickness of the hydrate stability field can be estimated from the subbottom depth of the BSR. In distinct areas, which correspond to the flanks of topographic highs, a shallowing of the base of the hydrate zone is observed. Furthermore, the occurrence of the BSR is restricted to fractured and accreted sediments or to the vicinity of faults. In contrast, the BSR is not present within bedded hemipelagic deposits.

If active fluid transport is required to form a BSR, some characteristics of the BSR may be used to reveal information about the regional distribution of permeability. Since a clear BSR is present, diffuse fluid migration is inferred for the pervasively fractured sediments of the accretionary wedge. In contrast, low permeable bedded

deposits inhibit vertical fluid flow and a BSR may only form in the vicinity of faults, where gas is locally provided at sufficient rates. The elevation of the BSR beneath the flanks of topographic highs is interpreted as a local disturbance of the thermal gradient, which is related to an increase of hydraulic conductivity within the deforming and outcropping sediments and a subsequent guided rise of warm fluids. A positive heatflow anomaly of 10-15% may be estimated for the area of maximum BSR elevation.

At the surface of bedded sediments, zones of high seafloor reflectivity are observed, which do not reveal a sharp base and are thicker than the commonly observed hemipelagic layers. Further, the occurrences of the BSR and the highly reflective zones appear to be mutually exclusive. Only few exceptions are present in areas, where basins of bedded deposits are shallower than the BSR.

Zones of high reflectivity at the seafloor are attributed to early diagenetic processes, which cement the surface sediments and increase the acoustic impedance. The precipitates probably consist of methane derived carbonates, associated with fault controlled fluid upflow through the low permeable beds of hemipelagic deposits.

In conclusion, the diffuse seepage in the vicinity of ODP Sites 889 and 890 is superimposed by at least two additional types of confined fluid release. One is guided through pathways within deforming outcrops, the second is related to faults in low permeable environments. Both types, however, are most likely related to episodic fault displacement and flow rates are considered to be time-variable. Associated time scales are not necessarily identical, although the same tectonic event may locally initiate both types of fluid expulsion. The thickness of highly reflective surface zones as well as the heatflow anomaly, which has not yet

been dissipated by thermal diffusion, may be indicative for the duration and intensity of flow.

Acknowledgements

R/V „Sonne“ cruise SO111 was supported by the German Ministry of Science and Technology (BMBF, Grant No. 03G111B). Support for this work was provided through the Graduiertenkolleg „Stoff-Flüsse in marinen Geosystemen“ at the University of Bremen, Germany, which was funded by the Deutsche Forschungsgemeinschaft (DFG). Careful reviews by R.D. Hyndman and N. Kukowski as well as helpful comments by G.D. Spence clearly improved this manuscript. M. Gutowski assisted with the picking of BSR arrivals. We thank the captain and crew of R/V „Sonne“ for excellent technical support during cruise SO111.

References

Bohrmann G, Greinert J, Suess E, Torres M (1998) Authigenic carbonates from the Cascadia subduction zone and their relation to gas hydrate stability. Geology 26: 647-650

Bray CJ, Karig DE (1985) Porosity of sediments in accretionary prisms and some implications for dewatering processes. J Geophys Res 90: 768-778

Calvert AJ, Clowes RM (1991) Seismic evidence for the migration of fluids within the accretionary complex of western Canada. Can J Earth Sci 28: 542-556

Carson B, Seke E, Paskevich V, Holmes ML (1994) Fluid expulsion sites on the Cascadia accretionary prism: Mapping diagenetic deposits with processed GLORIA imagery. J Geophys Res 99: 11959-11969

Carson B, Westbrook GK (1995) Modern fluid flow in the Cascadia accretionary wedge: A synthesis. In: Westbrook GK, Carson B, Musgrave RJ, Suess E (eds.), Proc ODP Sci Res 146: College Station, TX (Ocean Drilling Program): 413- 421

Carson B, Screaton EJ (1998) Fluid flow in accretionary prisms: Evidence for focused, time-variable discharge. Rev Geophys 36: 329-351

Claypool GE, Kaplan IR (1974) The origin and distribution of methane in marine sediments. In: Kaplan IR (ed.) Natural gases in marine sediments. Plenum, New York, pp 99-139

Davis EE, Hyndman RD (1989) Accretion and recent deformation of sediments along the northern Cascadia subduction zone. Geol Soc Am Bull 101: 1465-1480

Davis EE, Hyndman RD, Villinger H (1990) Rates of fluid expulsion across the northern Cascadia accretionary prism: Constraints from new heat flow and multichannel seismic reflection data. J Geophys Res 95: 8869-8889

Davis EE, Becker K, Wang K, Carson B (1995) Long-term observations of pressure and temperature in hole 892B, Cascadia accretionary prism. In: Westbrook GK, Carson B, Musgrave RJ, Suess E (eds.), Proc ODP Sci Res 146: College Station, TX (Ocean Drilling Program): 299-311

Dillon WP, Paull CK (1983) Marine gas hydrates – II. Geophysical evidence. In: Cox JL (ed.) Natural gas hydrates: Properties, occurrences, and recovery. Butterworths, London, pp 73-90

Fink CR, Spence GD (1999) Hydrate distribution off Vancouver Island from multifrequency single-channel seismic reflection data. J Geophys Res 104: in press

Fisher AT, Hounslow MW (1990) Transient fluid flow through the toe of the Barbados accretionary complex: Constraints from Ocean Drilling Program Leg 110 heat flow studies and simple models. J Geophys Res 95: 8845-8858

Gornitz V, Fung I (1994) Potential distribution of methane hydrates in the world's oceans. Global Biogeochem Cycles 8: 335-347

Hyndman RD, Davis EE (1992) A mechanism for the formation of methane hydrate and seafloor bottom-simulating reflectors by vertical fluid expulsion. J Geophys Res 97: 7025-7041

Hyndman RD, Spence GD (1992) A seismic study of methane hydrate seafloor bottom-simulating reflectors. J Geophys Res 97: 6683-6698

Hyndman RD, Wang K, Yuan T, Spence GD (1993) Tectonic sediment thickening, fluid expulsion, and the thermal regime of subduction zone accretionary prisms: The Cascadia margin off Vancouver Island. J Geophys Res 98: 21865-21876

Kastner M, Kvenvolden KA, Whiticar MJ, Camerlenghi A, Lorenson TD (1995) Relation between pore fluid chemistry and gas hydrates associated with bottom-simulating reflectors at the Cascadia margin, Sites 889 and 892. In: Westbrook GK, Carson B, Musgrave RJ, Suess E (eds.), Proc ODP Sci Res 146: College Station, TX (Ocean Drilling Program): 175-187

Kopf A, Sample JC, Bauer P, Behrmann JH, Erlenkeuser H (1995) Diagenetic

carbonates from Cascadia margin: Textures, chemical compositions, and oxygen and carbon stable isotope signatures. In: Westbrook GK, Carson B, Musgrave RJ, Suess E (eds.), Proc ODP Sci Res 146: College Station, TX (Ocean Drilling Program):117-136

Kulm LD, Suess E (1990) Relationship between carbonate deposits and fluid venting: Oregon accretionary prism. J Geophys Res 95: 8899-8915

Kvenvolden KA (1988) Methane hydrate – A major reservoir of carbon in the shallow geosphere? Chem Geol 71: 41-51

Kvenvolden KA (1994) Natural gas hydrate occurrence and issues. New York Acad Sci Annals 715: 232-246

MacKay ME, Jarrard RD, Westbrook GK, Hyndman RD, Shipboard Scientific Party of Ocean Drilling Program Leg 146 (1994) Origin of bottom-simulating reflectors: Geophysical evidence from the Cascadia accretionary prism. Geology 22: 459-462

Minshull T, White R (1989) Sediment compaction and fluid migration in the Makran accretionary prism. J Geophys Res 94: 7387-7402

Moore JC, Orange D, Kulm LD (1990) Interrelationship of fluid venting and structural evolution: *Alvin* observations from the frontal accretionary prism, Oregon. J Geophys Res 95: 8795-8808

Moore JC, Vrolijk P (1992) Fluids in accretionary prisms. Rev. Geophys 30: 113-135

Moran K, Gray WGD, Jarrett CA (1995) Permeability and stress history of sediment from the Cascadia margin. In: Westbrook GK, Carson B, Musgrave RJ, Suess E (eds.), Proc ODP Sci Res 146: College Station, TX (Ocean Drilling Program): 275-280

Paull CK, Ussler II W, Borowski WS (1994) Sources of biogenic methane to form marine gas-hydrates, in situ production or upward migration? New York Acad Sci Annals 715: 392-409

Ritger S, Carson B, Suess E (1987) Methane-derived authigenic carbonates formed by subduction-induced pore-water expulsion along the Oregon/Washington margin. Geol Soc Am Bull 98: 147-156

Sample JC, Kopf A (1995) Isotope geochemistry of syntectonic carbonate cements and veins from the Oregon margin: Implications for the hydrogeologic evolution of the accretionary wedge. In: Westbrook GK, Carson B, Musgrave RJ, Suess E (eds.), Proc ODP Sci Res 146: College Station, TX (Ocean Drilling Program): 137-147

Shipboard Scientific Party (1994) Sites 889 and 890. In: Westbrook GK, Carson B, Musgrave RJ, et al., Proc ODP Init Repts 146: College Station, TX (Ocean

Drilling Program): 127-231

Singh SC, Minshull TA, Spence GD (1993) Velocity structure of a gas hydrate reflector. Science 260: 204-207

Sloan ED (1990) Clathrate hydrates of natural gases. Marcel Dekker, New York, pp 1-641

Smith WHF, Wessel P (1990) Gridding with continuous curvature splines in tension, Geophysics 55: 293-305

Spence GD, Minshull TA, Fink C (1995) Seismic studies of methane gas hydrate, offshore Vancouver Island. In: Westbrook GK, Carson B, Musgrave RJ, Suess E (eds.), Proc ODP Sci Res 146: College Station, TX (Ocean Drilling Program): 163-174

Stockwell JW (1997) Free software in education: A case study of CWP/SU: Seismic Un*x. The leading edge 16: 1045-1049

Suess E, Bohrmann G, von Huene R, Linke P, Wallmann K, Lammers S, Sahling H, Winckler G, Lutz RA, Orange D (1998) Fluid venting in the eastern Aleutian subduction zone. J Geophys Res 103: 2597-2614

Villinger H, Fahrtteilnehmer (1996) Fahrtbericht SO111. Berichte, Fachbereich Geowissenschaften, Universität Bremen, 97, pp 1-122

Yuan T, Hyndman RD, Spence GD, Desmons B (1996) Seismic velocity increase and deep-sea gas hydrate concentration above a bottom-simulating reflector on the northern Cascadia continental slope. J Geophys Res 101: 13655-13671

Figure captions

Fig. 1 Location of ODP sites, single channel seismic lines (Lines 1-7) and multi channel seismic lines (GeoB96-069, GeoB96-071, GeoB96-073). Bathymetry data were acquired with the Hydrosweep system onboard R/V Sonne (contour levels 40 m). The quadrangle indicates the working area.

Fig. 2 Line 5: **a:** Single channel seismic data reveal a strong bottom simulating reflector. **b:** Parasound data reveal discontinuous zones of high reflection amplitudes at the seafloor. Vertical exaggeration (VE) for all figures is given for a velocity of 1750 m/s.

Fig. 3 Line GeoB96-071: **a:** Multi channel seismic data. The double reflection of the BSR is caused by the inverted wavelet of GI-Gun #2 for a negative reflection coefficient. **b:** Parasound data. High seafloor reflectivity appears to be restricted to slope basin deposits.

Fig. 4 Line 1: **a:** Single channel seismic data. The BSR is missing within basins of bedded deposits but is strong within the pervasively fractured sediments of the accretionary prism. **b:** Parasound data. High seafloor reflectivity appears to be restricted to slope basin deposits (compare to Figure 3).

Fig. 5 Close-up of the northern half of Line 3: **a:** Single channel seismic data. The BSR is observed in the vicinity of a fault. **b:** Parasound data.

Fig. 6 Close-up of the Parasound record of Line GeoB96-071 (compare to Figure 3). Zones of high reflectivity follow the layering in the top portion, but do not reveal a sharp base. Furthermore, they are covered by a 0.5-5 m thick transparent sediment drape.

Fig. 7 Seafloor topography provided by the Hydrosweep system (contour levels 40 m), related to hand-picked locations of **a:** a distinct BSR in GI-Gun data, and **b:** zones of high near surface reflectivity in Parasound data. A comparison suggests that the presence of a BSR and of high reflectivity zones is mutually exclusive.

Fig. 8 Close-up of Line 5 (compare to Figure 2), focusing on the BSR (lower panel) and the seafloor reflection (middle panel) after leveling the first arrivals. Parasound data (upper panel) show the location of high reflectivity zones and the original topography. The BSR is locally elevated and reveals a gap of 300 m width.

Fig. 9 a: Topography of the BSR. Positive values represent an elevation above an average depth below seafloor in two-way reflection time (contour levels 10 ms). White circles mark areas where a BSR is observed. **b:** Topography of the BSR related to bathymetry (contour levels 40 m, compare to Figure 1). The maximum elevation of about 50 ms TWT is found at the northern flanks of topographic highs.

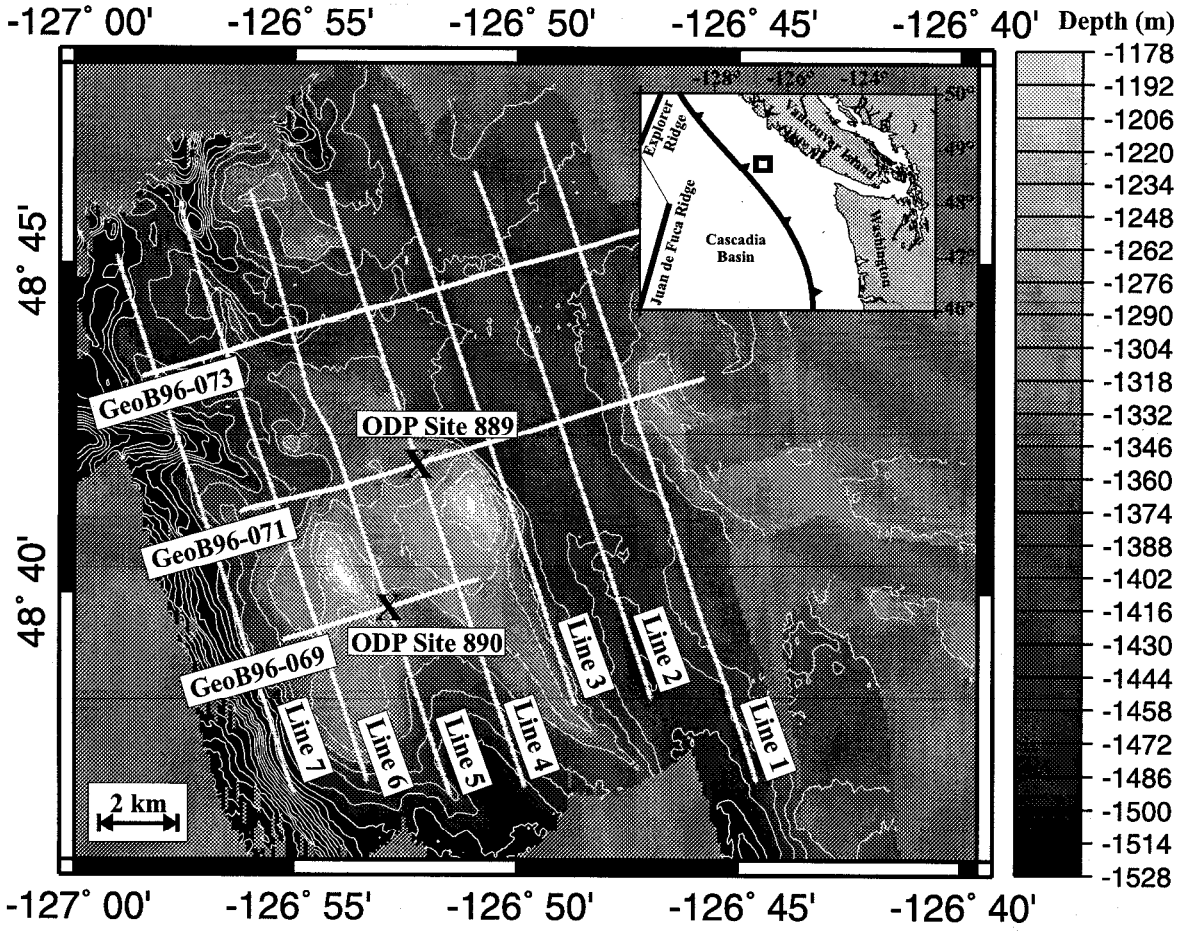
-127° 00'
-126° 55'
-126° 50'
-126° 45'
-126° 40'
Depth (m)
-1178
-1192
-1206
-1220
-1234
-1248
-1262
-1276
-1290
-1304
-1318
-1332
-1346
-1360
-1374
-1388
-1402
-1416
-1430
-1444
-1458
-1472
-1486
-1500
-1514
-1528
48° 45'
48° 40'
GeoB96-073
GeoB96-071
GeoB96-069
ODP Site 889
ODP Site 890
Line 1
Line 2
Line 3
Line 4
Line 5
Line 6
Line 7
2 km
Explorer Ridge
Juan de Fuca Ridge
Cascadia Basin
Vancouver Island
Washington

Fig. 1

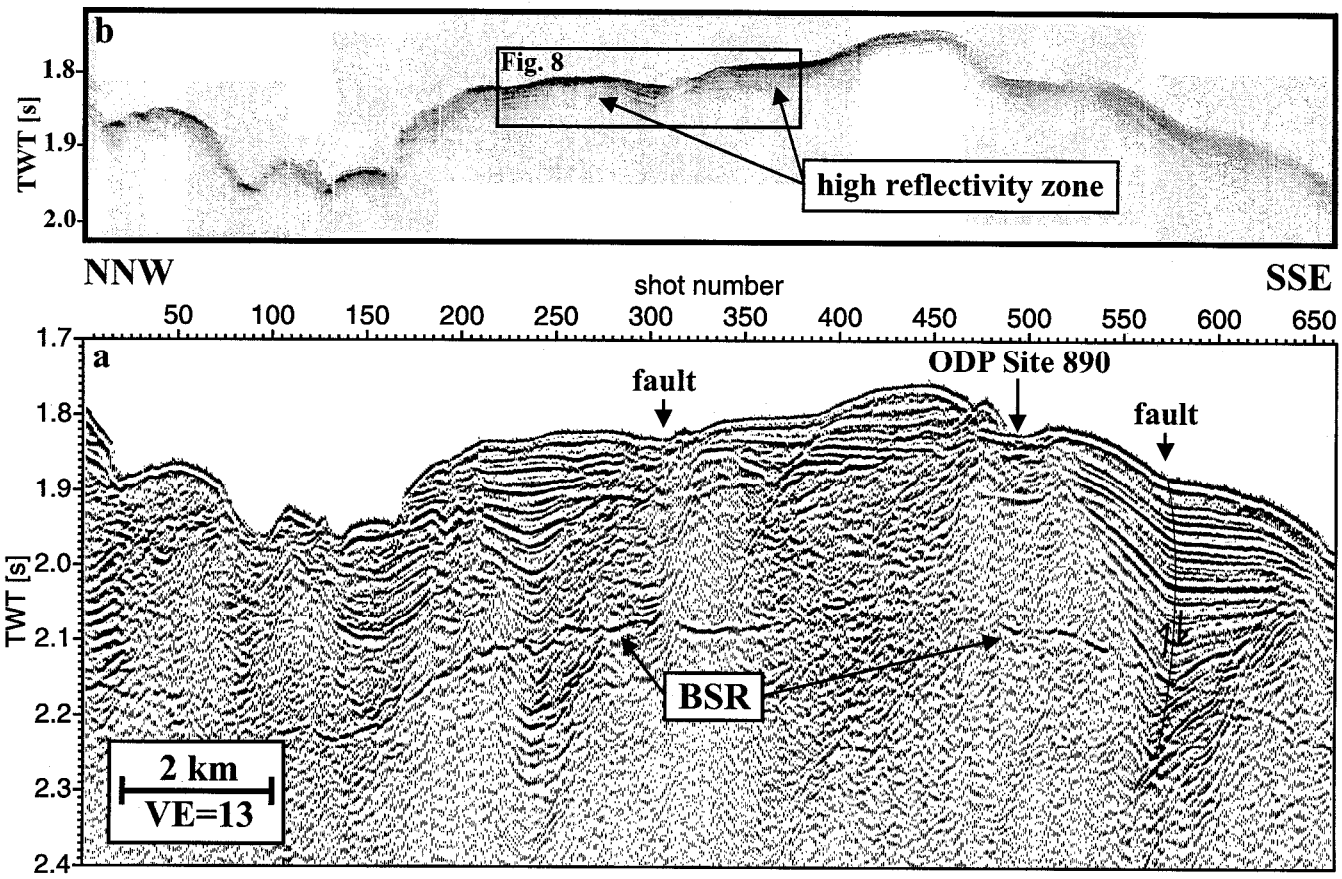
b
Fig. 8
high reflectivity zone
TWT [s]
1.8
1.9
2.0
NNW
shot number
SSE
50
100
150
200
250
300
350
400
450
500
550
600
650
a
fault
ODP Site 890
fault
BSR
2 km
VE=13
1.7
1.8
1.9
2.0
2.1
2.2
2.3
2.4

Fig. 2

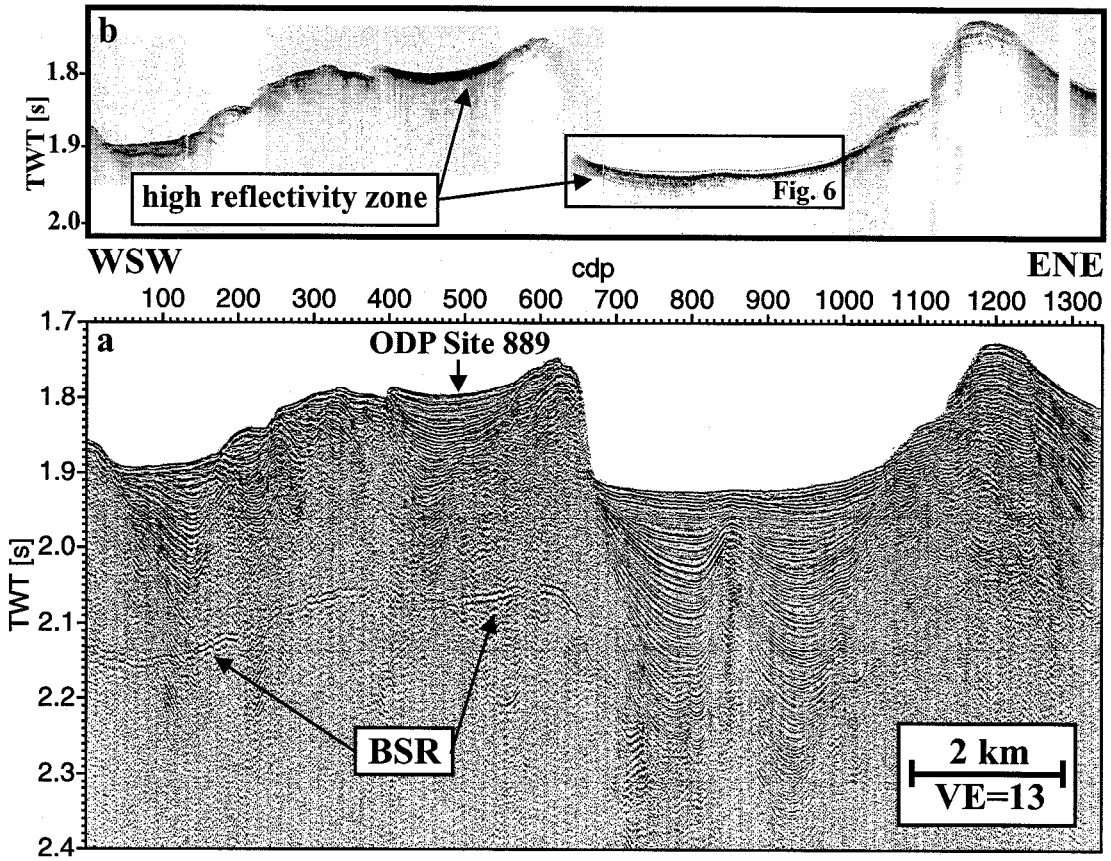
b
1.8
1.9
2.0
TWT [s]
high reflectivity zone
Fig. 6
WSW
cdp
ENE
100 200 300 400 500 600 700 800 900 1000 1100 1200 1300
a
ODP Site 889
1.7
1.8
1.9
2.0
2.1
2.2
2.3
2.4
TWT [s]
BSR
2 km
VE=13

Fig. 3

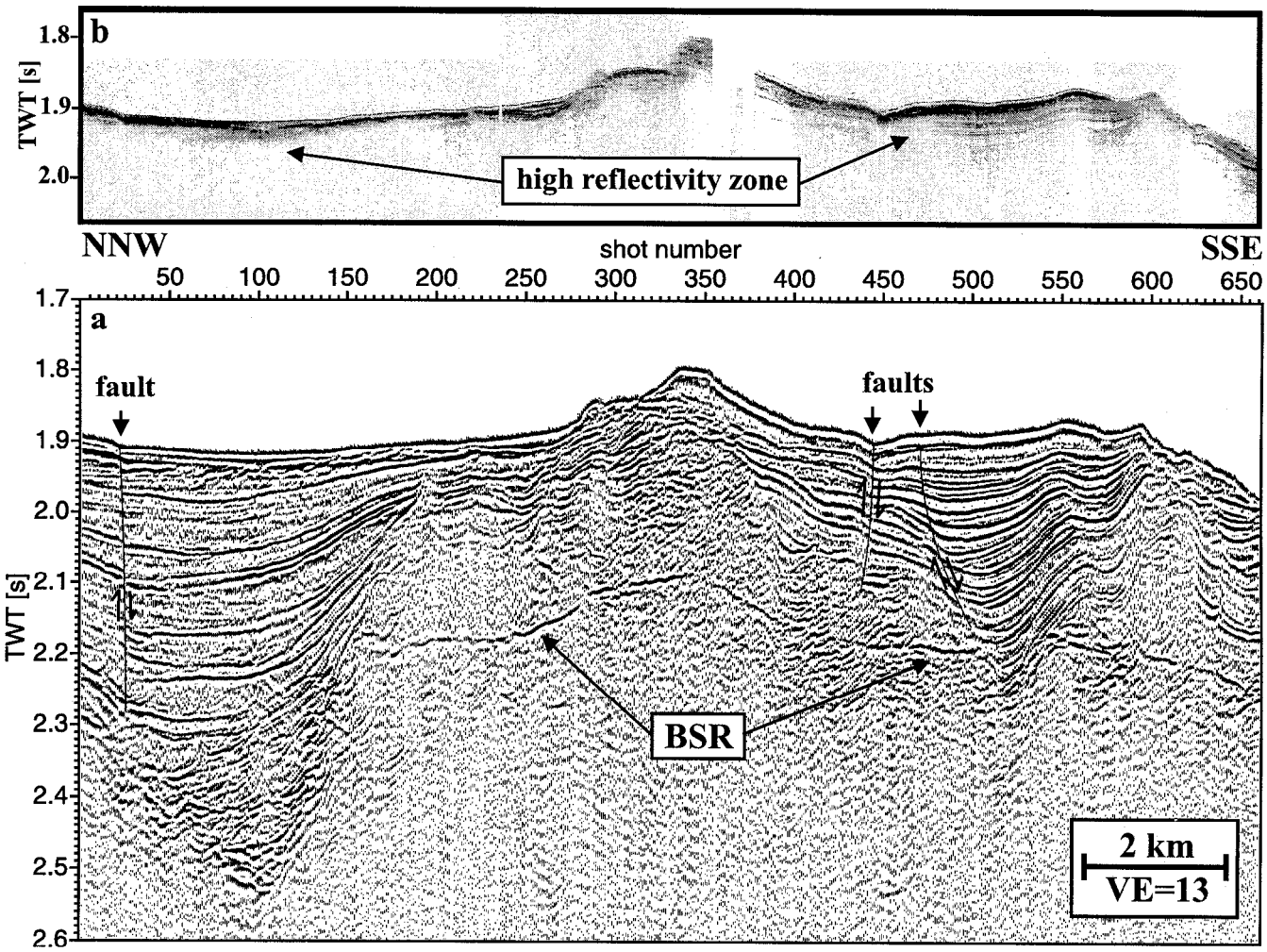
b
1.8
1.9
2.0
TWT [s]
high reflectivity zone
NNW
shot number
SSE
50
100
150
200
250
300
350
400
450
500
550
600
650
a
1.7
1.8
1.9
2.0
2.1
2.2
2.3
2.4
2.5
2.6
TWT [s]
fault
faults
BSR
2 km
VE=13

Fig. 4

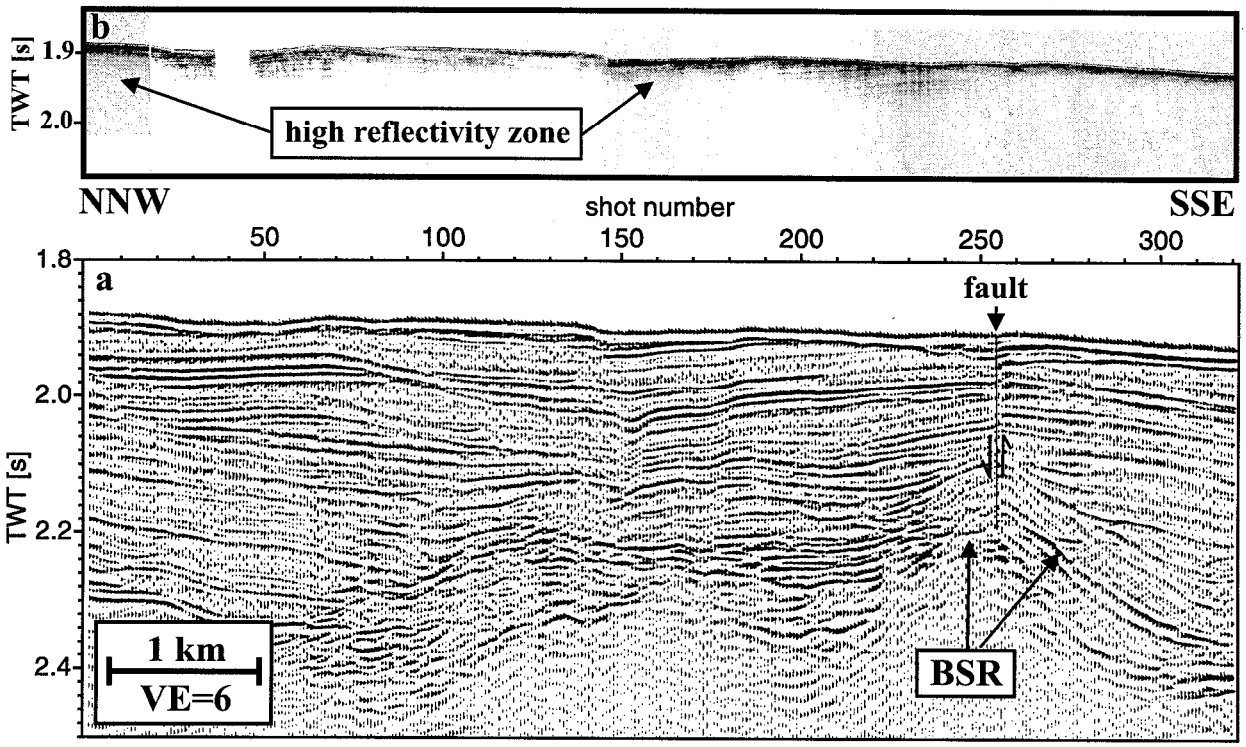
b
TWT [s]
1.9
2.0
high reflectivity zone
NNW
shot number
SSE
50
100
150
200
250
300
1.8
a
fault
2.0
TWT [s]
2.2
1 km
VE=6
2.4
BSR

Fig. 5

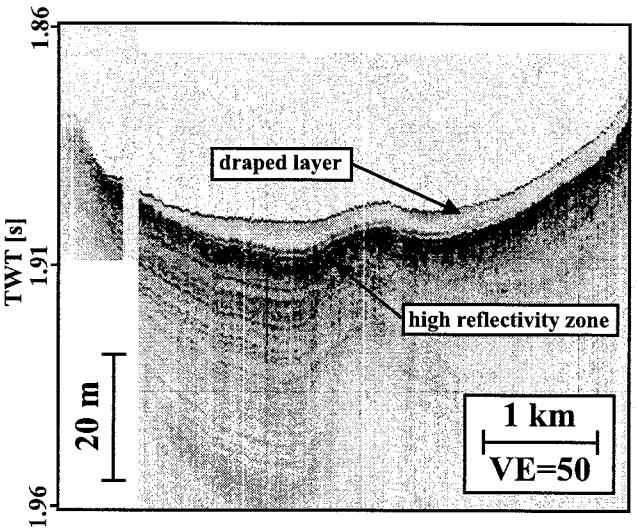
1.86
TWT [s]
1.91
1.96
draped layer
high reflectivity zone
20 m
1 km
VE=50

Fig. 6

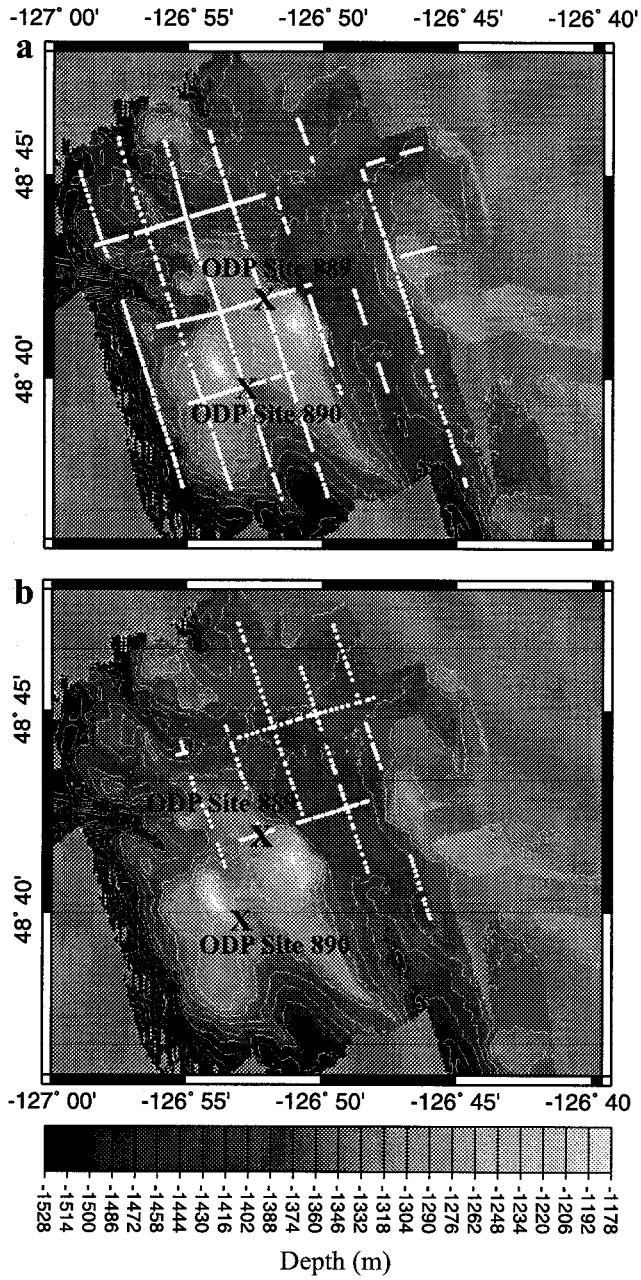
-127° 00'
-126° 55'
-126° 50'
-126° 45'
-126° 40'
a
48° 45'
48° 40'
ODP Site 889
ODP Site 890
b
48° 45'
48° 40'
ODP Site 889
ODP Site 896
-127° 00'
-126° 55'
-126° 50'
-126° 45'
-126° 40
-1528
-1514
-1500
-1486
-1472
-1458
-1444
-1430
-1416
-1402
-1388
-1374
-1360
-1346
-1332
-1318
-1304
-1290
-1276
-1262
-1248
-1234
-1220
-1206
-1192
-1178
Depth (m)

Fig. 7

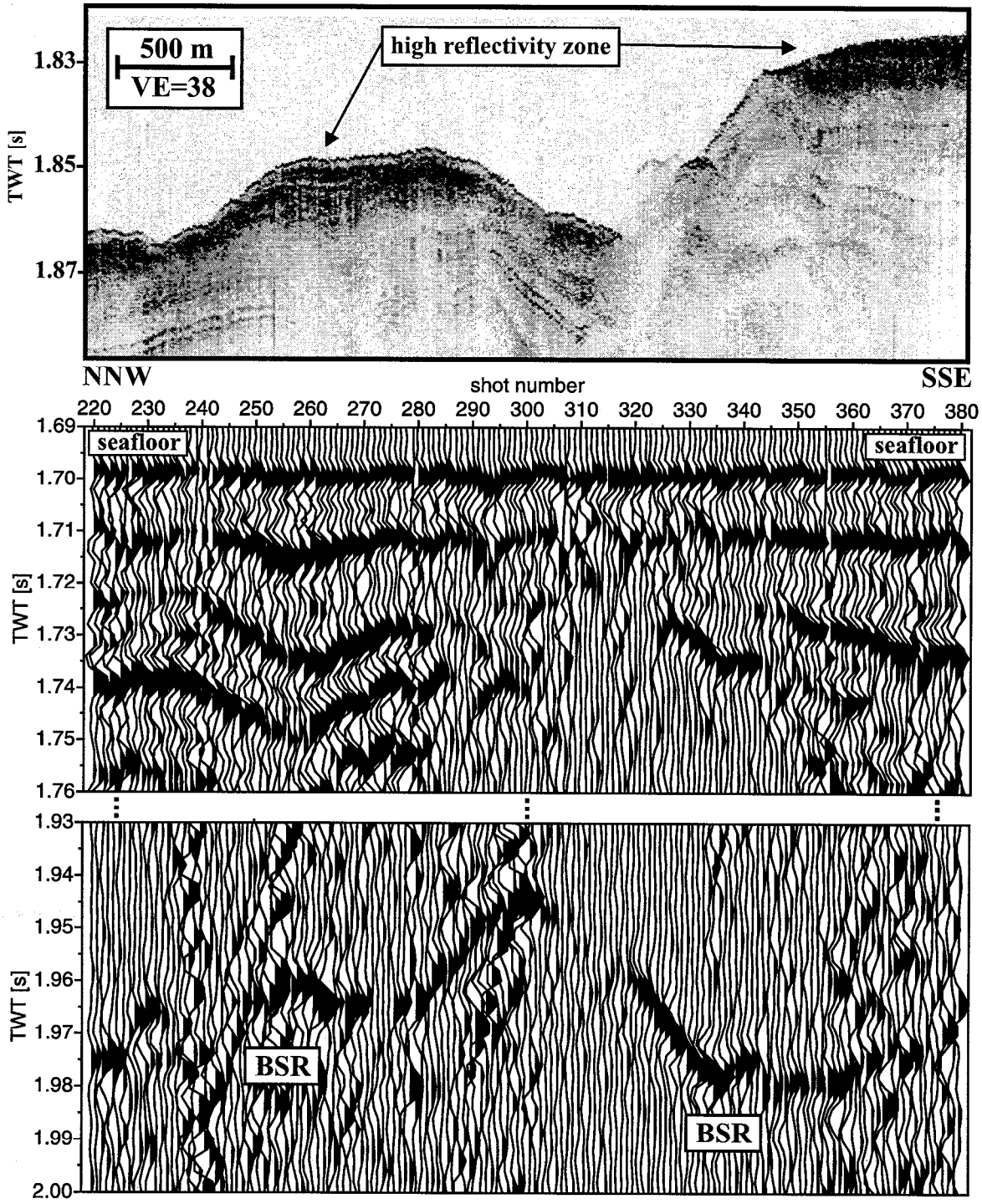
500 m
VE=38
high reflectivity zone
1.83
1.85
1.87
TWT [s]
NNW
SSE
shot number
220 230 240 250 260 270 280 290 300 310 320 330 340 350 360 370 380
seafloor
seafloor
1.69
1.70
1.71
1.72
1.73
1.74
1.75
1.76
1.93
1.94
1.95
1.96
1.97
1.98
1.99
2.00
BSR
BSR

Fig. 8

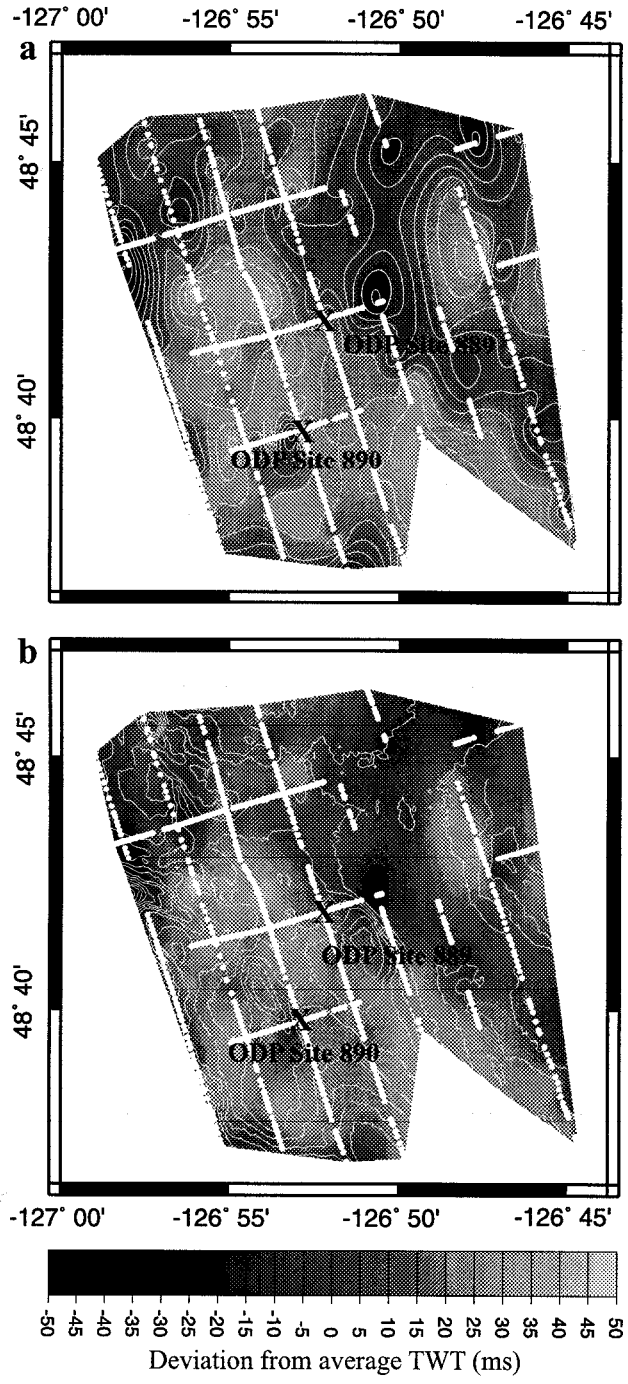
-127° 00'
-126° 55'
-126° 50'
-126° 45'
a
48° 45'
48° 40'
ODP Site 889
ODP Site 890
b
48° 45'
48° 40'
ODP Site 889
ODP Site 890
-127° 00'
-126° 55'
-126° 50'
-126° 45'
-50 -45 -40 -35 -30 -25 -20 -15 -10 -5 0 5 10 15 20 25 30 35 40 45 50
Deviation from average TWT (ms)

Fig. 9

Table 1

Source	Type	Frequency (Hz)	Processing
GI-Gun #1	scs	50-150 (bandwidth)	filter, migration
GI-Gun #2	mcs	100-400 (bandwidth)	filter, CDP-stack, migration
Parasound	echosounder	4000 (dominant freq.)	filter